

Article

Channel Morphology Change after Restoration: Drone Laser Scanning versus Traditional Surveying Techniques

Jonathan P. Resop ^{1,*}, Coral Hendrix ², Theresa Wynn-Thompson ² and W. Cully Hession ²¹ Department of Geographical Sciences, University of Maryland, College Park, MD 20740, USA² Department of Biological Systems Engineering, Virginia Tech, Blacksburg, VA 24060, USA; tthompson@vt.edu (T.W.-T.); chession@vt.edu (W.C.H.)

* Correspondence: resop@umd.edu

Abstract: Accurate and precise measures of channel morphology are important when monitoring a stream post-restoration to determine changes in stability, water quality, and aquatic habitat availability. Practitioners often rely on traditional surveying methods such as a total station for measuring channel metrics (e.g., cross-sectional area, width, depth, and slope). However, these methods have limitations in terms of coarse sampling densities and time-intensive field efforts. Drone-based lidar or drone laser scanning (DLS) provides much higher resolution point clouds and has the potential to improve post-restoration monitoring efforts. For this study, a 1.3-km reach of Stroubles Creek (Blacksburg, VA, USA), which underwent a restoration in 2010, was surveyed twice with a total station (2010 and 2021) and twice with DLS (2017 and 2021). The initial restoration was divided into three treatment reaches: T1 (livestock exclusion), T2 (livestock exclusion and bank treatment), and T3 (livestock exclusion, bank treatment, and inset floodplain). Cross-sectional channel morphology metrics were extracted from the 2021 DLS scan and compared to metrics calculated from the 2021 total station survey. DLS produced 6.5 times the number of cross sections over the study reach and 8.8 times the number of points per cross section compared to the total station. There was good agreement between the metrics derived from both surveying methods, such as channel width ($R^2 = 0.672$) and cross-sectional area ($R^2 = 0.597$). As a proof of concept to demonstrate the advantage of DLS over traditional surveying, 0.1 m digital terrain models (DTMs) were generated from the DLS data. Based on the drone lidar data, from 2017 to 2021, treatment reach T3 showed the most stability, in terms of the least change and variability in cross-sectional metrics as well as the least erosion area and volume per length of reach.

Keywords: stream restoration; channel morphology; lidar; surveying; drone laser scanning; UAVs

Citation: Resop, J.P.; Hendrix, C.; Wynn-Thompson, T.; Hession, W.C. Channel Morphology Change after Restoration: Drone Laser Scanning versus Traditional Surveying Techniques. *Hydrology* **2024**, *11*, 54. <https://doi.org/10.3390/hydrology11040054>

Academic Editor: Jarosław Chormański

Received: 1 March 2024

Revised: 3 April 2024

Accepted: 8 April 2024

Published: 10 April 2024



Copyright: © 2024 by the authors. Licensee MDPI, Basel, Switzerland. This article is an open access article distributed under the terms and conditions of the Creative Commons Attribution (CC BY) license (<https://creativecommons.org/licenses/by/4.0/>).

1. Introduction

Federal, state, and local agencies in the United States and other countries spend significant time, money, and resources on stream restoration efforts, with over USD 1 billion spent annually in the USA [1]. For example, in the Chesapeake Bay watershed, more than 1400 km of restoration is planned to be completed by 2025 for a total cost of around USD 500 million [2]. The term “stream restoration” is used for many different techniques and practices, such as native riparian forest establishment, channel reconstruction, and flow control, as well as dam removal [3].

A common restoration goal is to improve long-term channel stability [2,4]. Researchers rely on morphology metrics, such as channel width-to-depth ratio and cross-sectional area, to monitor change and assess project success [5–7]. Government agencies have used the consistency of these metrics over time as criteria for evaluating stream stability. For example, the Virginia Department of Environmental Quality (VDEQ), based on a template produced by the US Army Corps of Engineers (USACE), defined a series of “performance standards” for restoration projects that included criteria such as the change in width-to-depth ratio should be between 1.3 and 0.7 and the cross-sectional area cannot increase or decrease more

than 25% over a 10-year monitoring period [8]. However, it is important to note that while some agencies have placed an emphasis on stability as a way to reduce streambank erosion, researchers have noted that “locking in place” should not be a strict goal, since streams naturally experience some level of migration [9,10]. However, in spite of the existence of these criteria, many restoration projects are not properly monitored or evaluated for effectiveness due to the lack of time, money, resources, and/or personnel [11,12]. In addition, many projects are only monitored for a few years at most or not evaluated at all [13,14]. Ultimately, more monitoring and evaluation are needed to learn from successes and failures [2,15].

Traditional methods for monitoring stream change after restoration, such as surveying repeat cross-sectional profiles with a total station or using erosion pins for measuring streambank retreat, have many limitations. These techniques can result in bias depending on how the operator chooses to locate the surveyed points and are prone to measurement errors [16]. In addition, these methods have the potential to physically disturb the stream being surveyed [17]. Traditional surveying methods are limited by the number of point measurements collected, which results in a coarse representation of channel morphology [18]. Repeat surveys with a total station also require a series of permanently marked cross-sections (often steel rebar driven into the ground) which can be lost over time or move due to freeze–thaw processes [19].

To improve on the limitations of traditional surveying, remote sensing technologies, both passive and active, have been utilized to survey streams. Satellite imagery has been used to monitor planimetric changes in river morphology, such as changes in centerline location, channel width, and surface area [20–22]. Passive remote sensing with satellite or aerial imagery allows one to survey large reaches over multiple decades. However, by nature, imagery is designed to collect spectral data, not elevation data. It can be difficult to produce accurate measures of channel depth from a raster-based image; however, it is possible under certain conditions, depending on the shallowness and turbidity of the stream as well as the resolution of the images [23,24].

Remote sensing using unoccupied aerial vehicles (UAVs), such as drone-based imagery, also known as structure-from-motion (SfM), has been successfully utilized for surveying stream channels and classifying floodplain vegetation [25], quantifying channel change after flooding events [26,27], monitoring channel morphology post-restoration [28], and measuring streambank erosion [29]. However, passive remote sensing technologies such as imagery and SfM have difficulty penetrating dense vegetation canopy to survey ground topography [30,31].

Active remote sensing using lidar has an advantage over imagery since it directly measures elevation in the form of 3-D point clouds. Aerial laser scanning (ALS) with piloted aircraft has been used to measure channel morphology, generate stream networks, and quantify channel change at resolutions typically around 0.5 to 1 m [32–35]. However, due to the altitude and scan angle of ALS, properly scanning the sides of streambanks can be difficult, which are critical components of stream profiles [36]. Terrestrial laser scanning (TLS) mounted on a tripod has been used to measure streambank retreat rates as well as channel erosion and deposition volume at a high spatial resolution (0.02 to 0.05 m) [18,37]. However, the TLS platform is best suited for smaller extents and can be cumbersome when surveying larger stream reaches [38].

Advances in UAV payloads including drone-based lidar, also known as UAV-based lidar or drone laser scanning (DLS), have demonstrated the potential of DLS to avoid many of the limitations of other remote sensing technologies [39]. Since drones fly at a lower altitude than piloted aircraft, DLS can produce much higher density point clouds than ALS [36]. Additionally, the lower flight altitude allows DLS to more precisely survey streambanks compared to ALS [36]. Since drones provide a very mobile and versatile platform, DLS can scan over a larger area of interest than TLS on a stationary tripod [18,36]. In many ways, DLS provides the best of both technologies: the scanning extent of ALS with the resolution of TLS [36,39].

Drone laser scanning has only recently been applied to measure channel morphology. Backes et al. [40] scanned a reach downstream of a glacier in Austria using both drone-based SfM as well as drone-based lidar to measure changes in river morphology over multiple years through a 3-D surface change analysis. They found DLS produced a much higher point density (556 points/m²) of the stream channel compared to SfM (190 points/m²) [40]. Islam et al. [41] scanned a 1.2 km reach of the lower Asahi River in Japan using a green laser-based UAV to survey bathymetry (up to 1 or 2 m in depth depending on the turbidity) as well as floodplain topography and vegetation, but this technology is still relatively new and not yet widely available. These studies note the advantage of DLS for surveying large stream reaches at high resolution. However, little research has been carried out to directly compare cross sections measured using traditional surveying methods to those extracted using DLS.

The objectives of this study were as follows: (1) to scan a reach of Stroubles Creek, which underwent a restoration in 2010, multiple times with drone-based lidar (in 2017 and 2021); (2) to compare cross-sectional metrics (e.g., channel width and depth) calculated from a traditional total station survey in 2021 with those derived from drone lidar; and (3) to quantify the changes in channel morphology post-restoration (from 2017 to 2021) using drone lidar data and compare the results between three restoration treatment areas.

2. Materials and Methods

2.1. Study Area

Stroubles Creek is a small, mixed bedrock and gravel-bed stream located downstream of Virginia Tech's campus in Blacksburg, VA, USA. Its watershed has an area of 15 km² and consists of developed land use (e.g., the campus, downtown area, and suburban housing) and agricultural land use (e.g., pastures) [42]. The stream has undergone extensive human modification, such as channel straightening, and part of the stream is piped under the university campus and within the town. Due to a history of non-point source pollutant loading from both urban and agricultural sources, Stroubles Creek is on the Environmental Protection Agency's 303(d) list of impaired streams for aquatic life impairment with sediment identified as the primary stressor [43].

The study area is a 1.3 km reach of Stroubles Creek, which is the research site for the StREAM Lab at Virginia Tech [44]. This reach underwent a stream restoration that was completed in May 2010 [42]. The restoration project divided the reach into three different restoration treatment areas (Figure 1) [42,45]. For the first treatment (T1; 0.5 km), the only action performed was livestock (i.e., cattle) exclusion from the riparian area (Figure 2a). In the second treatment (T2; 0.6 km), in addition to livestock exclusion, the banks were reshaped to a stable grade (3:1) and native woody vegetation was planted (Figure 2b). In the third treatment (T3; 0.3 km), in addition to livestock exclusion and planting vegetation, an inset floodplain was sized to ensure entrainment of sand-sized bed material annually and the D50 of the riffles on average every five years (Figure 2c). While the active restoration activities formally ended in 2010, long-term goals included continually monitoring post-restoration changes in channel morphology through topographic surveys (Figure 1) [42].

This reach of Stroubles Creek has been the site of multiple DLS studies. Resop et al. [36] found the higher resolution of DLS (point density = 455 points/m²) to be better suited for scanning the sides of streambanks and providing detail about the channel profile than traditional ALS (point density = 4 points/m²). Prior et al. [46] used DLS and SfM to quantify hydraulic roughness, while Resop et al. [47] demonstrated how repeat DLS surveys can produce high-resolution measures of annual and seasonal vegetation change. In addition, Christensen et al. [48] utilized a combination of DLS and surveying data to compare floodplain connectivity across the three treatment areas. These studies concluded that DLS is well suited for measuring stream and floodplain topography and has the potential for monitoring morphological changes along Stroubles Creek.

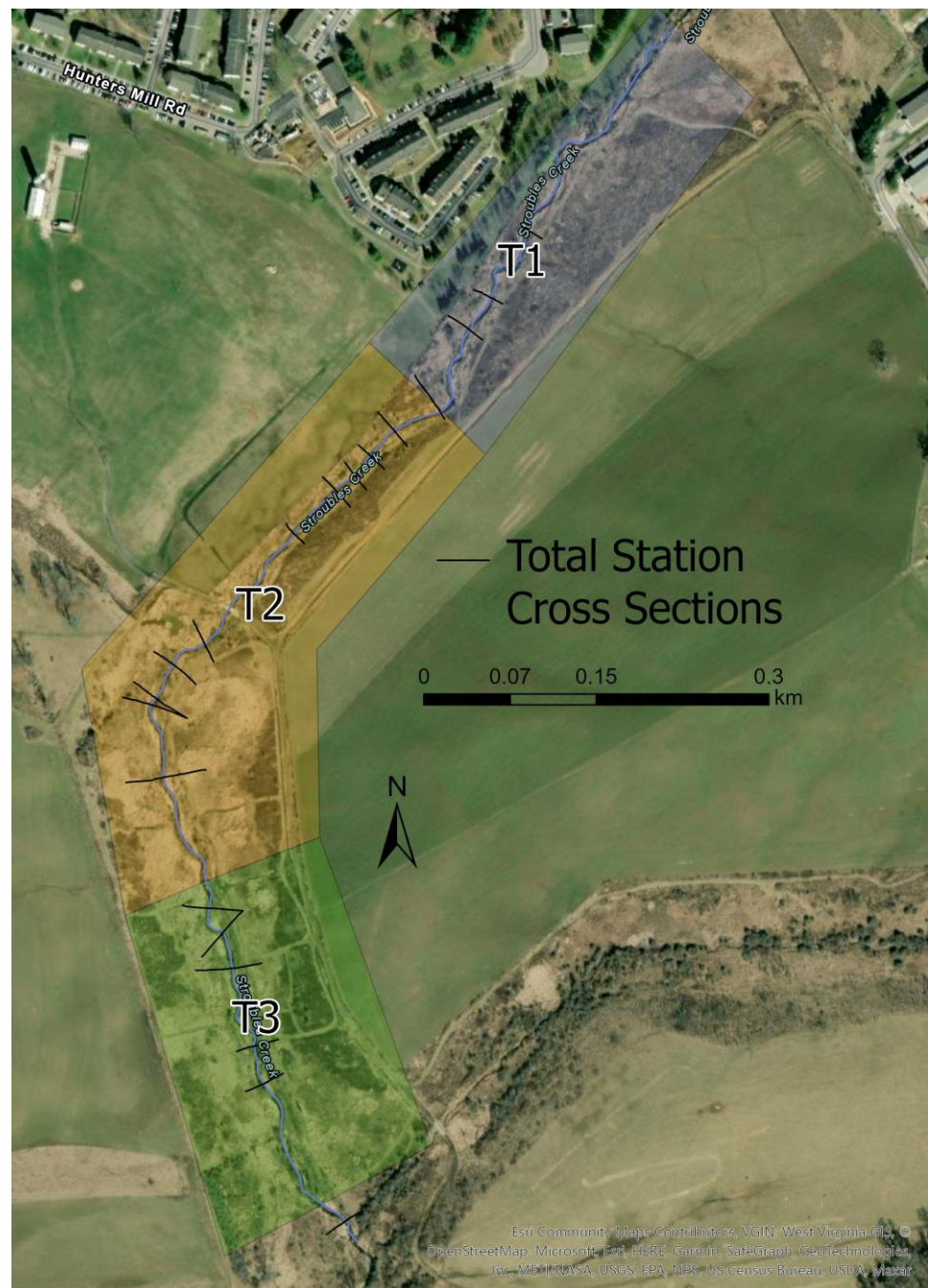


Figure 1. The three stream restoration treatments applied to Stroubles Creek: T1 (livestock exclusion), T2 (livestock exclusion and bank treatment), and T3 (livestock exclusion, bank treatment, and inset floodplain). Twenty cross sections over the study reach were surveyed in 2010 and 2021 via total station. The background image is ArcGIS Pro World Imagery, dated February 2020.

2.2. Data Collection and Processing

2.2.1. Total Station Survey Data Collection

The study reach was surveyed in 2010 with a Topcon GR-3 GNSS receiver (Livermore, CA, USA) (RTK accuracy: 10 mm horizontal, 15 mm vertical) after the restoration project was completed. The survey included 20 cross sections measured irregularly down the 1.3 km reach, with 4 located in T1, 10 in T2, and 6 in T3 (Figure 1). The ends of each cross section were marked with rebar. Each cross section was about 30 to 50 m in length (average 42.3 m) and focused on measuring key components of the stream channel morphology, such

as the top of bank (the point where stream flow spills out onto the floodplain), streambank, thalweg (the point of lowest elevation), streambed, and significant changes in elevation. On average, 46 points were measured per cross section (Table 1). The same twenty cross sections were resurveyed in 2021 with a Trimble R10 GNSS receiver (Westminster, CO, USA; RTK accuracy: 8 mm horizontal, 15 mm vertical) using a similar approach [49].



Figure 2. Photos of Stroubles Creek at each of the three stream restoration treatment reaches: (a) T1 (livestock exclusion; taken April 2022), (b) T2 (livestock exclusion and bank treatment; taken April 2022), and (c) T3 (livestock exclusion, bank treatment, and inset floodplain; taken December 2022).

Table 1. Cross section summary statistics for each surveying method over each treatment reach, where T1 was livestock exclusion, T2 was livestock exclusion and bank treatment, and T3 was livestock exclusion, bank treatment, and inset floodplain.

Surveying Method (Years)	Number of Cross Sections				Average Cross Section Length (m)	Average Points per Cross Section
	T1	T2	T3	Total		
Total station (2010, 2021)	4	10	6	20	42.3	46
Drone laser scanning (2017, 2021)	42	55	33	130	40.6	407

2.2.2. Drone Lidar Data Collection

The DLS system used for this study was a Pulse Aerospace (now AeroVironment) Vapor35 drone (Simi Valley, CA, USA) equipped with a YellowScan Surveyor Core lidar (Montferrier-sur-Lez, France). The lidar system had a near-infrared (NIR) laser with a wavelength of 905 nm and a pulse rate of 300 kHz. Additional details about the DLS system can be found in Resop et al. [36]. The drone was flown at an altitude of 20 m for all

surveys [47] (Figure 3). At this altitude, previous studies with this DLS system reported point densities over 400 points/m² [36,47].



Figure 3. (a) The drone taking off for a test flight in September 2021 and (b) the drone flying over Stroubles Creek for a survey in December 2021.

With the lidar payload, the UAV system had a maximum flight time of 40 min [36]. Since the entire study reach was too large to scan in a single flight, each survey was split into two flights: the northern reach and the southern reach. The point cloud data from both flights were merged together into a single dataset during post-processing. Two separate DLS surveys of the study reach were performed: 2017 (March for the north and April for the south) and 2021 (November for the north and December for the south). After data collection, the point clouds were pre-processed, georeferenced, and exported to LAS files for analysis. The 2021 dataset is publicly available on OpenTopography [50].

2.2.3. Drone Lidar Data Processing

The DLS flights were merged into a single point cloud for each survey (2017 and 2021) and processed as LAS datasets using ArcGIS Desktop 10.6 and ArcGIS Pro 3.1 (Redlands, CA, USA). The datasets were projected to NAD 83 UTM Zone 17N and vertical datum NAVD 88. Both DLS surveys consisted of similar scan extents over the study area (Figure 4) and the point clouds had similar densities (Table 2).

Table 2. Raw point statistics of the two drone lidar surveys performed for the study area.

Lidar Survey Year	Point Count	Point Spacing (m)	Point Density (pt/m ²)
2017	90,427,968	0.047	455
2021	92,460,991	0.046	472

The 2017 DLS point cloud was classified for a previous study as ground, unassigned, vegetation, building, and noise [36]. The 2021 DLS dataset was classified using a similar process in ArcGIS. The “Classify LAS Ground” tool was first used to classify ground points using its standard ground detection algorithm. The “Classify LAS by Height” tool was then used to classify the remaining points as either unassigned (height above ground < 0.1 m) or vegetation. The unassigned class represented points uncertain to be ground or vegetation due to the precision of the lidar system [51,52]. Points representing built structures, such as the concrete bridge in the middle of the reach and the three wooden bridges used for water quality measurements, were manually classified as building points by carefully identifying and selecting the points representing built structures in the point cloud.

During processing of the 2017 DLS dataset, Resop et al. [36] observed that two types of misclassifications commonly resulted from the classification algorithms. First, ground

points representing the streambank with a sharp gradient could be misclassified as vegetation. Second, vegetation points hanging over the stream could be misclassified as ground. These misclassifications have been noted as limitations of classifying high-resolution DLS point clouds in complex environments such as riverscapes using algorithms traditionally applied to lower-resolution ALS data [36]. As a result of these misclassifications, the points along the channel, which were critical for this study, required manual verification to ensure they were correctly classified. This verification was carried out for the 2017 dataset in a previous study [36] and was similarly performed here for the 2021 dataset.



Figure 4. The scan extents of the two drone lidar surveys flown over the study area. The background image is ArcGIS Pro World Imagery, dated February 2020.

After georeferencing and classifying the point clouds, it was observed that the 2017 and 2021 DLS point clouds were not properly aligned in the same coordinate system. A bias was observed between the two datasets, particularly for fixed structures like bridges. To correct this issue, the 2017 dataset was aligned to the 2021 dataset using a similar approach as Resop et al. [47]. The “Iterative Closest Point” tool in CloudCompare 2.10 (<https://www.cloudcompare.org/> accessed on 1 March 2024) was used to transform the 2017 DLS dataset to minimize the difference between it and the 2021 DLS dataset using built structures (i.e., one concrete bridge and three wooden bridges) as control points.

2.2.4. Generating Cross Sections from Drone Lidar Data

After the DLS point clouds for 2017 and 2021 were classified and verified, they were rasterized to produce digital terrain models (DTMs) representing the bare earth surface. This process was performed on the 2017 dataset by Resop et al. [36] using ArcGIS and repeated here for the 2021 dataset. First, the lidar datasets were filtered to select only ground and unassigned points, which were the points most likely to represent the bare earth surface. The “LAS Dataset to Raster” tool was then used to bin the point clouds to a 0.1 m raster based on the minimum elevation per pixel and a simple linear interpolation to fill in voids, such as the gap resulting from the stream surface. The DTMs were clipped to the scan extent (Figure 4) to remove interpolation artifacts outside of the boundary.

Cross sections were extracted from the 0.1 m DTMs using ArcGIS. A polyline representing the stream center for Stroubles Creek was manually delineated from the 2017 DTM. The “Generate Points Along Lines” tool was used to define a set of points every 10 m along the stream center from the top of the study reach to the bottom. A 20 m buffer was created around the stream center and cross-sectional lines were manually drawn tangential to the stream flow at each point to create a set of cross sections about 40 m in length (average 40.6 m) every 10 m down the reach. In total, 130 cross sections were generated for the study area: 42 for T1, 55 for T2, and 33 for T3 (Figure 5). The “Stack Profile” tool was used to extract the elevations from the 2017 and 2021 DTMs to the cross sections. The result was a set of cross sections for 2017 and 2021 with approximately the same resolution as the DTMs (0.1 m). On average, 407 points were extracted from the drone lidar DTMs per cross section (Table 1).

2.3. Deriving Channel Morphology Metrics

The channel morphology metrics for the 20 cross sections measured using a total station were calculated for a previous study into the long-term morphological changes of Stroubles Creek after restoration from 2010 to 2021 [49]. The top of bank was determined manually for each cross section as the point on the lower bank where there was a clear change in slope [49]. A constant top of bank elevation line was used for each cross section across both years (2010 and 2021). Autodesk Civil3D (San Rafael, CA, USA) was used to calculate the cross-sectional area, width, maximum depth, hydraulic depth, and width-to-depth ratio based on the top of bank line for each cross section for each year (Table 3) [49].

For the 130 cross sections generated using DLS, the top of bank was determined with ArcGIS. Similar to the traditionally surveyed cross sections, the top of banks for both streambanks were estimated as the point where there was a clear change in slope between the stream channel and floodplain [49]. A slope raster was derived from the DTM to assist with identifying the top of bank on both sides of the channel. The top of bank was identified on both streambanks to reduce bias in calculating channel width. The minimum top of bank elevation between both banks (i.e., the lower bank) was used to define the top of bank elevation line for each cross section, similar to Hendrix [49]. A separate top of bank elevation line was created for each cross section for both 2017 and 2021. Like before, this was carried out to reduce bias when measuring change between years. The cross-section profiles and top of bank points were imported into Python and a script was written to calculate the channel morphology metrics (i.e., cross-sectional area,

width, maximum depth, hydraulic depth, and width-to-depth ratio) for both 2017 and 2021 using the same definitions as for the total station cross sections (Table 3).

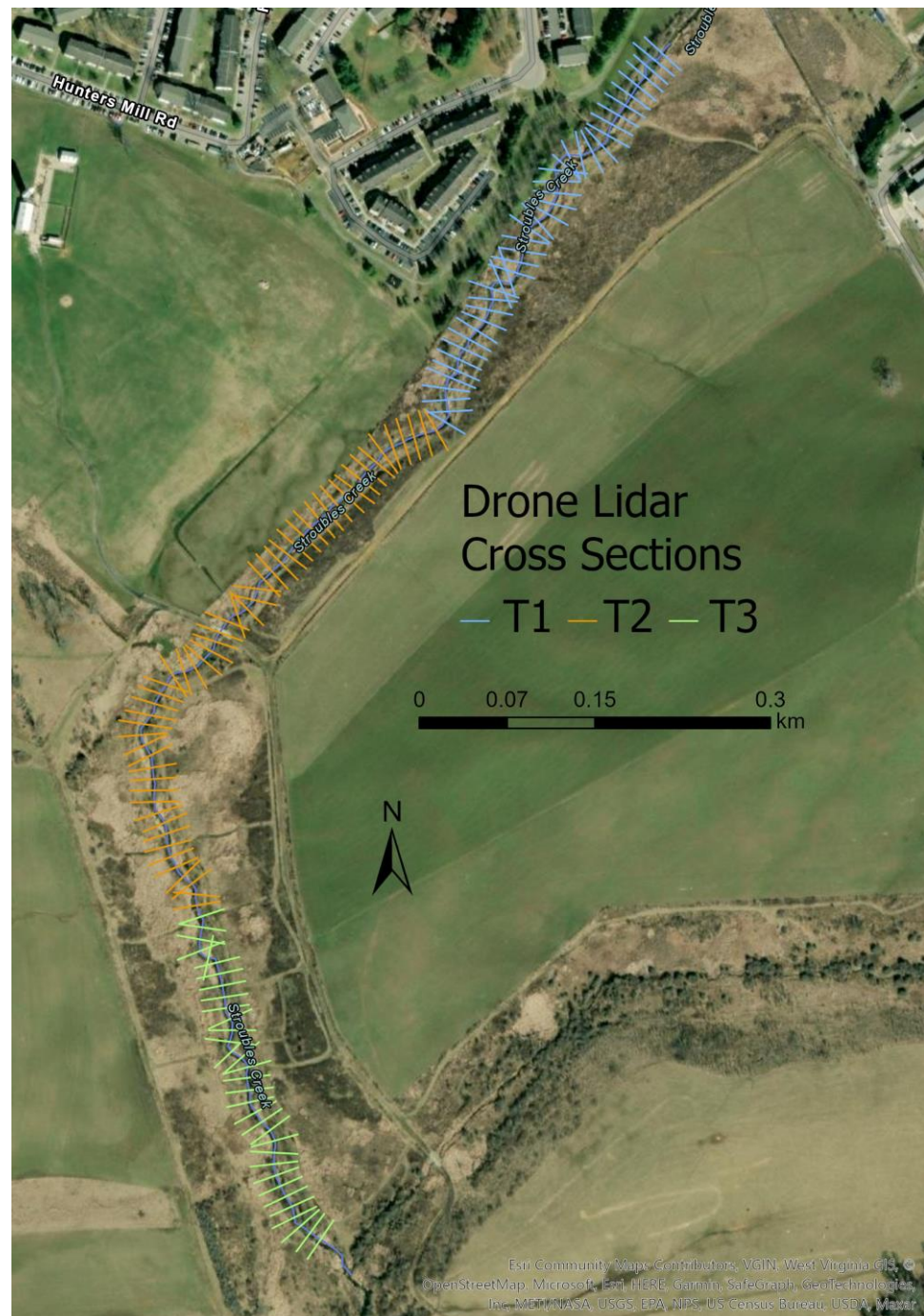


Figure 5. Cross sections generated every 10 m from the drone laser scanning (DLS) data for each treatment reach: T1 (livestock exclusion), T2 (livestock exclusion and bank treatment), and T3 (livestock exclusion, bank treatment, and inset floodplain). The background image is ArcGIS Pro World Imagery, dated February 2020.

It is important to note one key difference expected between the cross sections measured through traditional surveying and those produced with DLS; when surveying points in the field with a total station, the field crew can measure streambed points below the water surface. However, the cross sections generated from DLS were limited by the near-infrared

(NIR) laser of the lidar. Since NIR wavelengths are highly absorbed by water, lidar systems like the one used in this study are unable to reliably collect bathymetric data [36]. Both DLS surveys were conducted when Stroubles Creek was running at baseflow to attempt to minimize this issue. However, for the DLS surveys, the streambed had to be interpolated between the points collected at the bottom of the streambanks and the points on the bed not covered by water using a simple linear interpolation method.

Table 3. Channel morphology metrics for each cross section (adopted from Hendrix [49]).

Metric	Definition
Top of bank	The elevation where flow spills onto the floodplain
Cross-sectional area	The channel area under the top of bank elevation line
Channel width	The length of the top of bank elevation line
Maximum depth	The distance from the top of bank elevation line to the thalweg
Hydraulic depth	Cross-section area/channel width
Width-to-depth ratio	Channel width/hydraulic depth

2.4. Comparing Cross-Sectional Metrics between Total Station and Drone Lidar Data

A direct comparison between the total station and DLS data was only performed for 2021 since it was the only time both methods were utilized. For nineteen of the total station cross sections (one cross section in T3 was not covered by the DLS scan), the elevation from the lidar DTM was extracted to each total station point. Initially, the cross-sectional points between the two datasets were not aligned due to georeferencing differences. Six control points surveyed with the total station (one at the base station for each survey day) were used to calculate the elevation bias between the total station and lidar data. The control point bias ranged from -3.19 to 2.05 m. This bias was used to correct the elevation (Z) misalignment of the total station data. The total station cross sections were then shifted to correct translational (XY) misalignments. Once corrected, the mean bias difference ($DLS_z - TS_z$) and root mean squared difference ($RMSD_z$) were calculated between the 2021 total station points and the elevation extracted from the 2021 lidar DTM. Points were classified as bank or bed based on the streambank defined by the 2021 DLS data.

In addition to comparing the 2021 total station and drone lidar cross-sectional point elevations, the channel morphology metrics from Table 3 were compared for each cross section. At the locations of the 19 total station cross sections, 40 m long cross sections were manually delineated, sampled to 0.1 m resolution, and the 2021 lidar DTM elevation was extracted. The metrics were calculated for each DLS-derived cross section using a Python script and compared to the metrics calculated from the total station data by Hendrix [49]. The $RMSD$ and R^2 were calculated for each metric over the 19 cross sections to represent the level of agreement between the total station and DLS calculations.

2.5. Quantifying Channel Morphology Changes between Restoration Treatments

The change in Stroubles Creek's channel morphology from 2017 to 2021 was compared between the three treatment reaches based on the drone lidar data. Only change based on the DLS data was analyzed for this study; a change analysis from 2010 to 2021 based on the total station data was performed by Hendrix [49]. The change in each channel morphology metric (Table 3) was calculated as $metric_{2021} - metric_{2017}$ for each of the 130 DLS cross sections and summarized over each restoration treatment reach using box plots. The comparative analysis focused on the median and interquartile range (IQR) of the change in each cross-sectional metric between the three treatment reaches (T1, T2, and T3). Channel stability was defined as having the least change (median closer to zero) and least variability in cross section change (smaller IQR) over time.

A surface change analysis was also performed. The DEM of Difference (DoD) was calculated between the 2017 and 2021 drone lidar 0.1-m DTMs to identify the area and volume of erosion and deposition within the stream channel (defined by the 2017 top of bank) in each treatment reach. The DoD was defined as $DTM_{2021} - DTM_{2017}$ [53–56]. With

this convention, positive DoD values indicated deposition and negative values indicated erosion. The area of the channel consisting of the water surface (defined by the 2017 lidar gaps) was ignored to avoid any change resulting from interpolation artifacts. To determine significant change, a minimum level of detection (LoD) of 0.2 m was applied, which was used in similar studies [47,57], based on the lidar precision [52].

3. Results and Discussion

3.1. Comparing Cross-Sectional Metrics between Total Station and Drone Lidar Data

The mean elevation bias between the total station points and drone lidar DTM for 2021 was 0.093 m (Table 4), which indicates, on average, DLS over-estimated ground elevation compared to the total station. A slight over-estimation of elevation by the DLS was expected, since lidar pulses cannot perfectly penetrate riparian vegetation to measure ground (Figure 6). This bias was similar in magnitude to the laser precision and comparable to other studies [36,47,52,57]. The $RMSD_z$ was 0.176 m over all 867 total station points over 19 cross sections. There was no significant distinction in $RMSD_z$ between bank points (0.179 m) and bed points (0.168 m). Bed points consisted of streambed that was not covered by water as well as interpolated bed points.

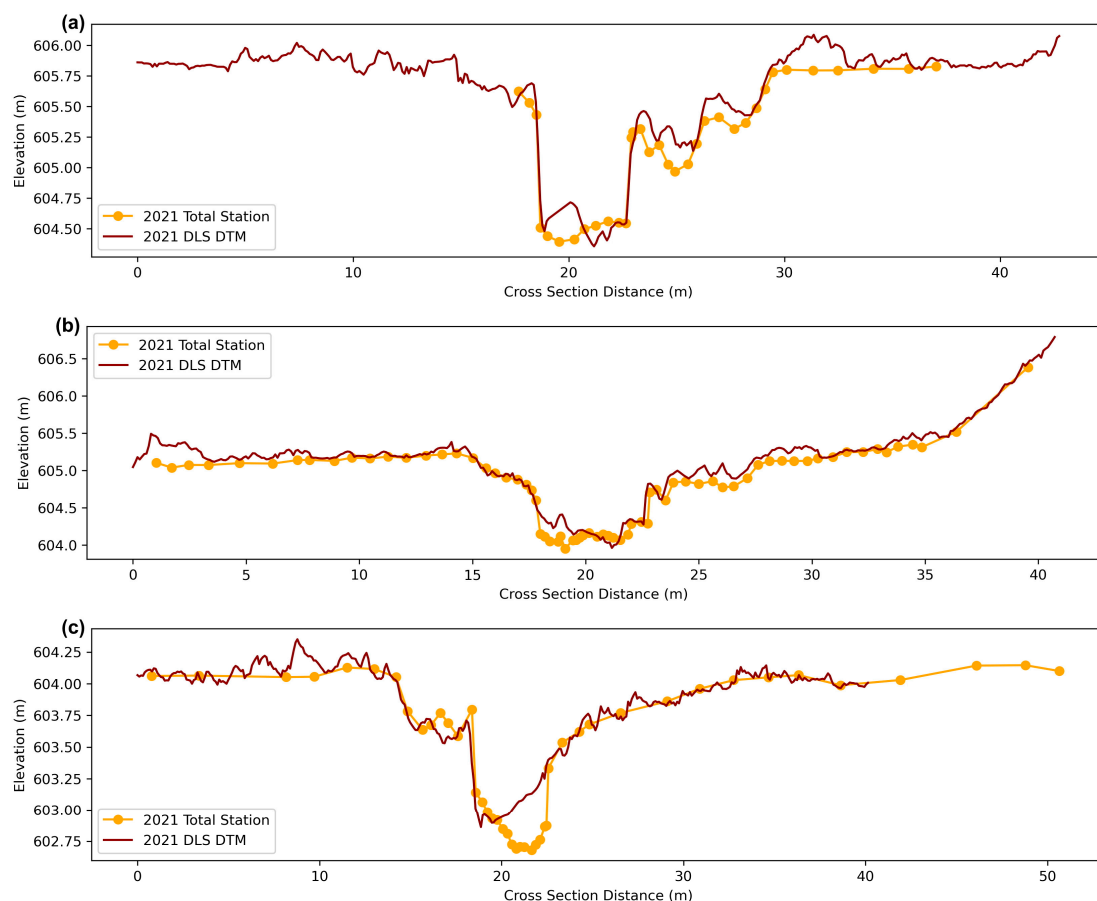


Figure 6. Example cross sections (in treatment reaches (a) T1, (b) T2, and (c) T3) comparing the total station points to the 0.1-m digital terrain model (DTM) produced with drone laser scanning (DLS).

The mean bias of the bank points (0.095 m) was slightly larger than the bed points (0.082 m) (Table 4). This indicates that the previously noted expectation, that the lidar bias would be greater under the water surface due to NIR absorption, was not as significant as anticipated and likely due to conducting the DLS surveys during baseflow when this reach of Stroubles Creek has an observed depth between 0.13 and 0.34 m [58]. For most cross sections, the bias under the water surface was within the overall bias observed between the

total station and DLS measurements (Figure 6). This bias was largest for pool cross sections and cross sections with overhanging vegetation. Both were the case for the example cross section in T3 shown in Figure 6c.

Table 4. Point elevation differences between the 2021 total station data and drone laser scanning (DLS) digital terrain model (DTM) summarized by point type (bank or bed) and treatment reach.

Total Station Point Type	Point Count	Mean Bias Difference (DLS _z – TS _z) (m)	Root Mean Square Difference (RMSD _z) (m)
All	867	0.093	0.176
Bank	681	0.095	0.179
Bed	186	0.082	0.168
T1	126	0.132	0.172
T2	496	0.116	0.184
T3	245	0.025	0.163

The mean bias over all points (bank and bed) decreased going from treatment reach T1 (0.132 m) to T2 (0.116 m) to T3 (0.025 m) (Table 4). The difference in elevation bias could be due to differences in riparian vegetation. Treatment reach T1 (livestock exclusion) consisted mostly of herbaceous vegetation while reaches T2 (livestock exclusion and bank treatment) and T3 (livestock exclusion, bank treatment, and inset floodplain) consisted mostly of woody vegetation. The denser vegetation in T1 was a likely cause for the higher elevation bias of the DLS data, but this should be explored more in future studies.

One of the advantages of DLS over traditional surveying was the effectiveness of repeat surveys over time. The original 2010 total station survey consisted of 30 cross sections; however, due to missing rebar markers, only 20 were located during the repeat survey in 2021, an effective rate of only 67% [49]. The DLS surveys were able to replicate 130 cross sections over the same stream reach from 2017 to 2021 with 100% effectiveness. Additionally, DLS produced a much higher resolution survey compared to the total station (Figure 6), with 6.5 times the number of cross sections and 8.8 times the number of points per cross section (Table 1).

The cross-sectional metrics derived from the 2021 DLS data showed good agreement with those calculated from the total station data over the 19 cross sections (Figure 7). In particular, the metrics with the best agreement were hydraulic depth ($R^2 = 0.693$), channel width ($R^2 = 0.672$), width-to-depth ratio ($R^2 = 0.605$), and cross-sectional area ($R^2 = 0.597$), which produced good correlations between the DLS and total station data. This indicates DLS accurately replicated the channel morphology measured with a total station. The metric with the worst agreement was maximum depth ($R^2 = 0.254$), which makes sense considering the limitation of DLS in scanning under water surfaces. The RMSD for maximum depth was 0.188 m, which was similar to the RMSD_z for streambed points (0.168 m) (Table 4) and within the range of the observed baseflow depth previously noted.

There is no evidence in the literature of any direct comparisons between DLS and traditional surveying for producing stream channel cross-sectional profiles; however, some analogs exist with other lidar platforms. Dietterick et al. [59] compared cross sections generated with ALS to ground surveying for a smaller, forested, mountain stream (watershed area = 5.26 km²) and reported agreements (R^2) of 0.653 for depth, 0.810 for width, and 0.859 for area. One important note is that Dietterick et al. [59] identified bankfull elevation in the field for their lidar profiles; however, in our study, the top of bank elevations were derived from the DLS DTMs using GIS, which likely resulted in additional uncertainty. Biron et al. [60] compared ALS to orthophotos for measuring channel width of two larger rivers and reported agreements (R^2) of 0.717 (watershed area = 59 km²) and 0.377 (watershed area = 1690 km²). Overall, the correlations we observed between the channel morphology metrics derived from DLS and total station surveying were in line with comparable studies with respect to the relative size of the study stream.

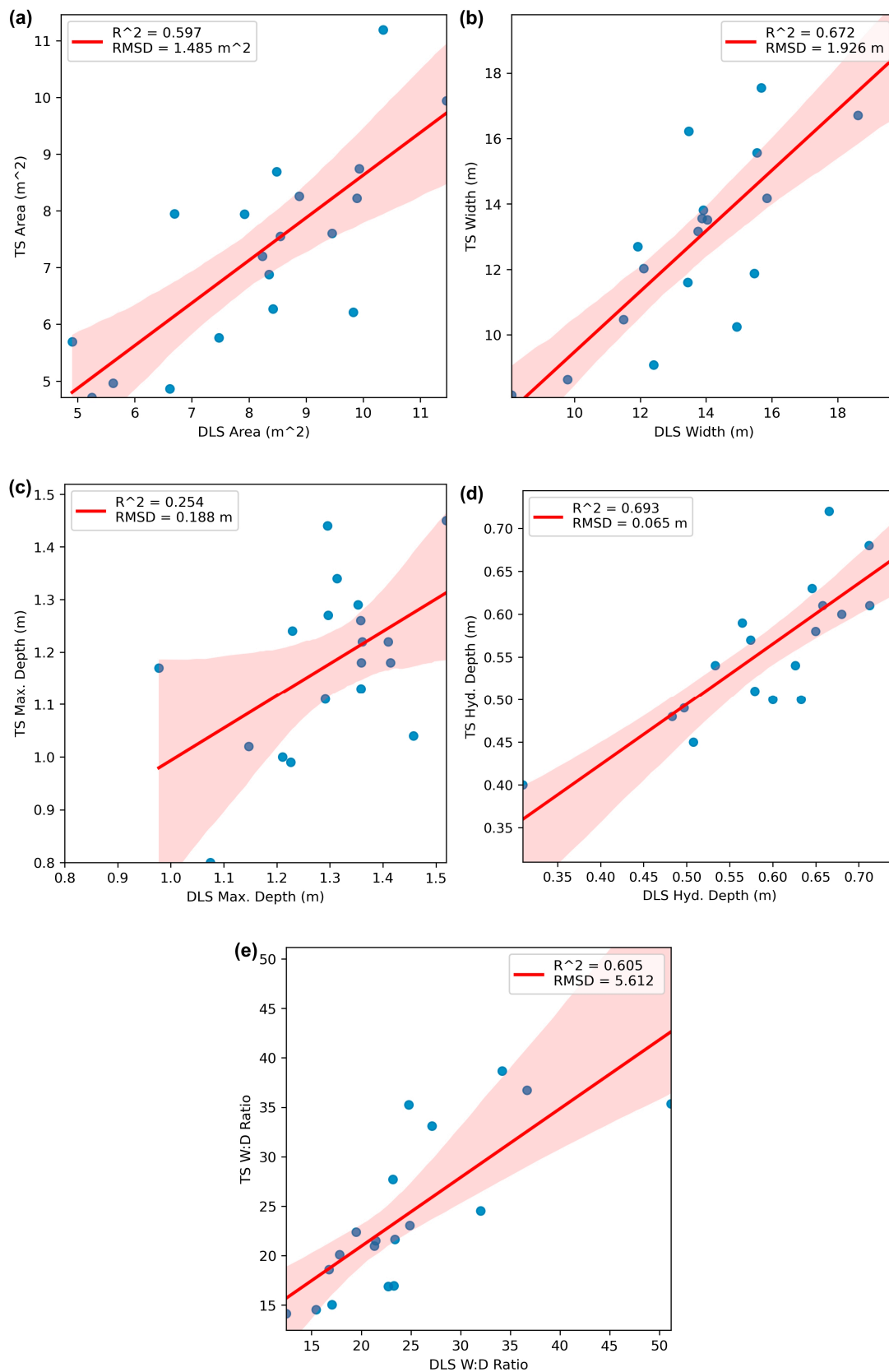


Figure 7. Correlation between the 2021 total station (TS) data (n = 19 cross sections; blue dots) and drone laser scanning (DLS) data represented by the linear regression best-fit line and 95% confidence interval (red area) for each of the channel morphology metrics ((a) cross-sectional area, (b) channel width, (c) maximum depth, (d) hydraulic depth, (e) width-to-depth ratio).

3.2. Quantifying Channel Morphology Changes between Restoration Treatments

For each of the 130 cross sections derived using DLS, the difference between 2017 and 2021 was calculated for each cross-sectional metric and summarized over the three treatment reaches to represent the channel morphology change over time (Figure 8). For cross-sectional area and channel width, treatment reach T3 demonstrated the most stability, in terms of a median change from 2017 to 2021 closer to zero, compared to the other two reaches. The median change in the cross-sectional area was negative in T1 (livestock exclusion; -0.488 m^2) but was positive in T2 (livestock exclusion and bank treatment; 0.845 m^2) and T3 (livestock exclusion, bank treatment, and inset floodplain; 0.230 m^2), indicating aggradation occurred in T1, while erosion was observed in T2 and T3. The median change in channel width was negative in T1 (-0.091 m), was positive in T2 (0.116 m), and was closest to zero in T3 (-0.042 m). Maximum depth increased consistently over all three reaches. The median change in maximum depth was 0.055 m for T1, 0.223 m for T2, and 0.111 m for T3. Treatment reach T1 had a median change closer to zero for both maximum depth and hydraulic depth, compared to the other two reaches.

Stability was also quantified as having a smaller IQR or variability in cross section change. A smaller variability means the cross sections within the treatment reach demonstrated similar changes in morphology from 2017 to 2021. Channel morphology generally increased in stability (i.e., decreased in variability) going from treatment reach T1 to T2 to T3. For example, the IQR for change in cross-sectional area decreased from T1 (2.031 m^2) to T2 (1.655 m^2) to T3 (1.371 m^2), channel width decreased from T1 (1.243 m) to T2 (1.010 m) to T3 (0.549 m), and width-to-depth ratio decreased from T1 (5.255) to T2 (4.246) to T3 (3.164) (Figure 8). Generally, T3 showed the least variability in cross section change for all channel morphology metrics except for maximum depth, which was more similar between the three treatment reaches (Figure 8).

As a specific comparison between treatments, the cross section with the median absolute change in channel width was selected for each reach (Figure 9). Absolute change was used to represent the magnitude of change and prevent positive and negative values from canceling out. The median absolute change in channel width was 0.633 m , 0.474 m , and 0.292 m for T1, T2, and T3, respectively. Generally, the absolute change in channel width decreased going from T1 to T2 to T3. These cross sections demonstrate that all three reaches showed considerable consistency between 2017 and 2021; however, reach T3 was more stable over this time period compared to the other two reaches.

The top of bank was located manually for both banks of each cross section and year to avoid bias in calculating the channel morphology metrics. By defining the left and right top of bank for each cross section based on the slope derived from the drone lidar DTM for each year, we argue this is the most objective way to calculate the top of bank from the DLS data. This resulted in slight differences in the top of bank elevation measured for each year. Between 2017 and 2021, the average absolute differences in top of bank elevations were 0.098 m for T1, 0.108 m for T2, and 0.068 m for T3. These differences were within the precision of the lidar and likely impacted by the riparian vegetation, as already discussed. The top of bank elevation differences were fairly low with respect to the average maximum channel depth in each reach, which was measured from the 2021 DLS data as 1.340 m for T1, 1.292 m for T2, and 1.248 m for T3.

In addition to comparing the DLS-derived cross sections, a 0.1 m DoD was calculated between the 2017 and 2021 DTMs, representing the areas of erosion and deposition over the study reach at high resolution (Figure 10). The stream showed classic patterns of erosion and deposition, particularly along bends and curves in the reach, as the channel migrated over time. Areas of erosion were more likely to occur along the outside of meander bends of the stream channel and areas of deposition were more likely along the point bars and on the inset floodplains. Particularly in treatment reach T1, the erosion areas demonstrated toe erosion and slumping of the upper bank, resulting in slump blocks in the channel. These results show evidence of bank retreat (through erosion) and bank advance (through

deposition) as the meander bends increased in amplitude following the historic channel straightening of Stroubles Creek.

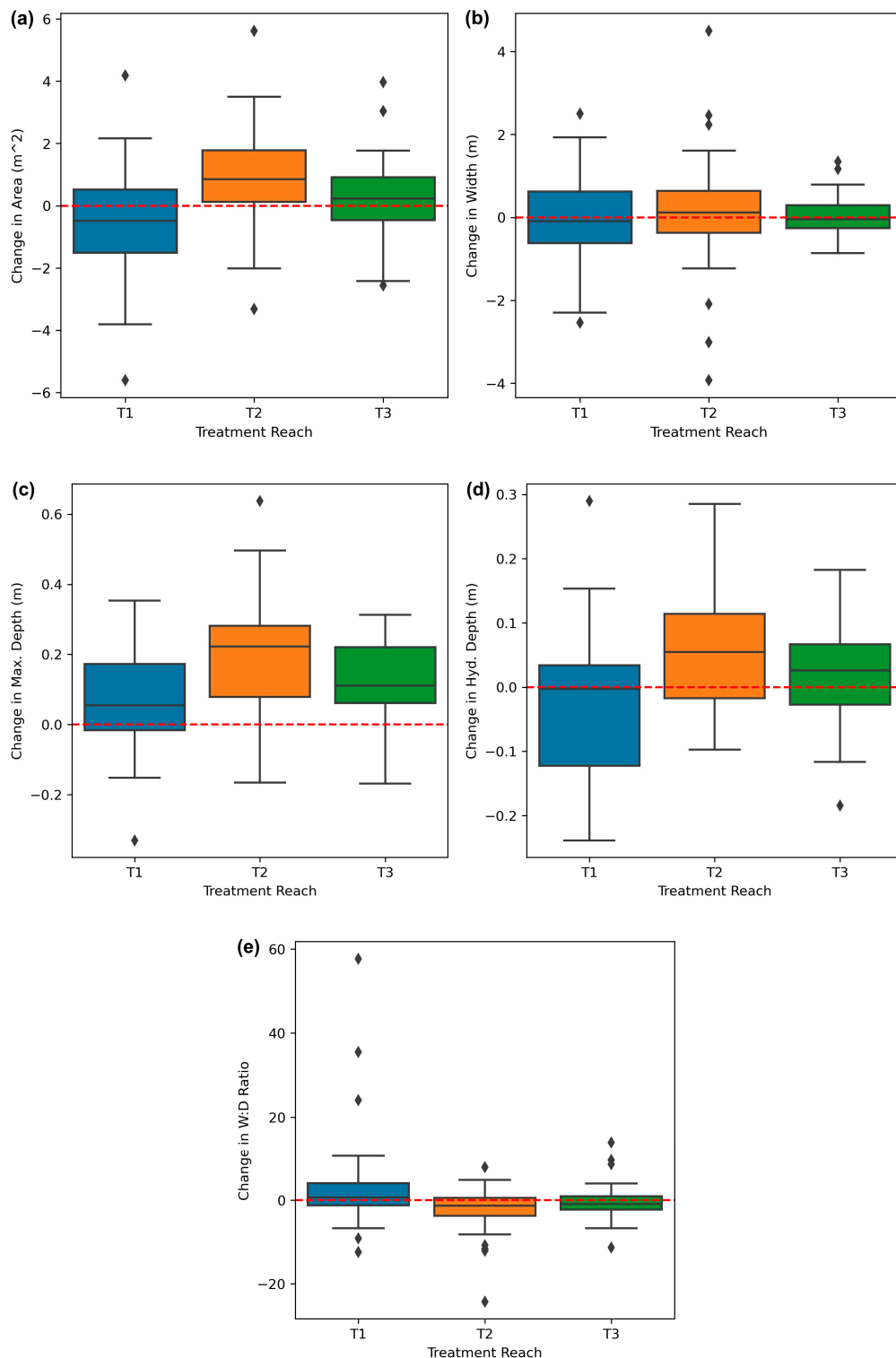


Figure 8. Change in cross-sectional metrics ((a) cross-sectional area, (b) channel width, (c) maximum depth, (d) hydraulic depth, (e) width-to-depth ratio), summarized by treatment reach, as measured by drone laser scanning (DLS) from 2017 to 2021 ($n = 130$ cross sections). The box represents the interquartile range (IQR), the line in the box represents the median, and the diamonds represent outliers. Change was calculated as 2021–2017.

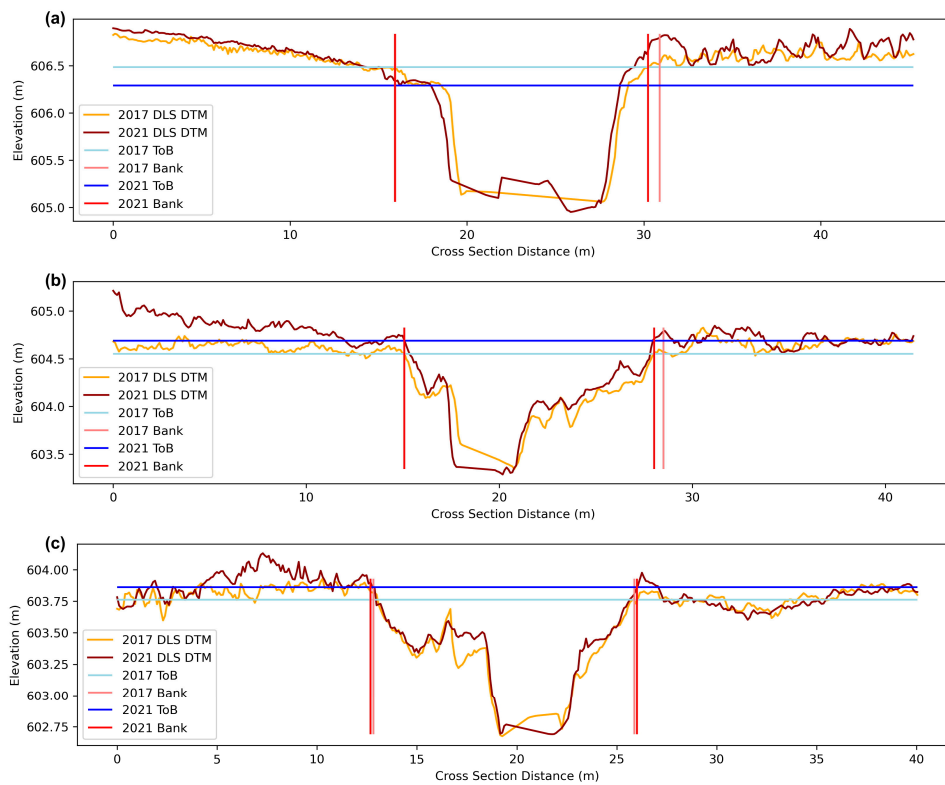


Figure 9. The cross section in each treatment reach ((a) T1, (b) T2, and (c) T3) with the median absolute change in width from 2017 to 2021 based on the drone laser scanning (DLS) data.

The change in area and volume was summarized for each of the treatment reaches (Table 5). Normalized by length, treatment reach T3 (livestock exclusion, bank treatment, and inset floodplain) had the least amount of erosion area ($1.481 \text{ m}^2/\text{km}$). The normalized erosion volume (in m^3/km) decreased as one traveled downstream from treatment reach T1 (0.914) to T2 (0.775) to T3 (0.422). A similar trend was observed for deposition, with less difference between T2 and T3.

Table 5. Summary of erosion and deposition by treatment reach, normalized by the reach length, as measured by drone laser scanning (DLS), based on the DEM of Difference (DoD) from 2017 to 2021 where elevation difference was calculated as 2021 – 2017.

Treatment Reach	Length (km)	Area per Length (m^2/km)		Volume per Length (m^3/km)	
		Erosion	Deposition	Erosion	Deposition
T1	0.429	2.683	11.759	0.914	4.207
T2	0.543	2.707	1.326	0.775	0.529
T3	0.324	1.481	1.697	0.422	0.548

Treatment reach T1 (livestock exclusion) had the largest normalized deposition volume ($4.207 \text{ m}^3/\text{km}$) and erosion volume ($0.914 \text{ m}^3/\text{km}$) compared to the other two reaches (Table 5). This difference might be due to T1 having a wider channel than T2 and T3, resulting in more potential for deposition. The average channel width for T1 was 17.0 m, compared to 13.4 m for T2 and 14.4 m for T3, based on the 2017 DLS dataset. The median change in channel width from 2017 to 2021 for T1 was -0.091 m , so deposition likely occurred in T1 as the channel continued to narrow from the original widening of Stroubles Creek caused by the cattle access [61]. At the time of the restoration in 2010, T1 was the most over-widened reach. The changes in T1 (e.g., decrease in width and high deposition) are likely due to multiple factors, including the fact it did not receive any treatment beyond

livestock exclusion. As a result, T1 has remained dominated by herbaceous vegetation and will likely have the smallest channel once Stroubles Creek ultimately “stabilizes”.

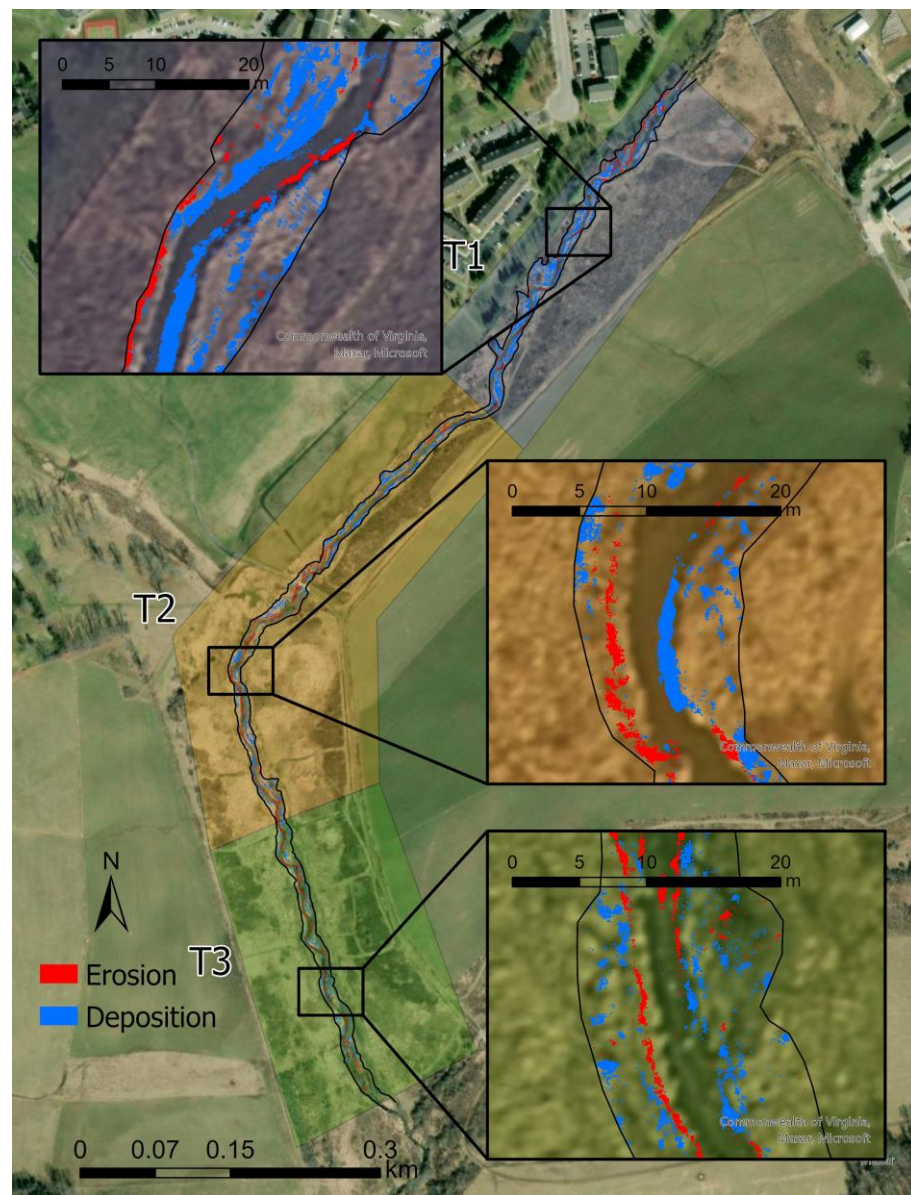


Figure 10. DEM of Difference (DoD) showing areas of erosion and deposition between 2017 and 2021 from drone laser scanning (DLS) 0.1 m digital terrain models (DTMs) over treatment reaches: T1 (livestock exclusion), T2 (livestock exclusion and bank treatment), and T3 (livestock exclusion, bank treatment, and inset floodplain). Elevation difference was calculated as 2021–2017. The background image is ArcGIS Pro World Imagery, dated February 2020.

In addition, treatment reach T1 mostly consisted of herbaceous vegetation while reaches T2 and T3 mostly consisted of woody vegetation. It was suspected that the herbaceous vegetation in T1 was more likely to trap sediment than the woody vegetation in T2 and T3, contributing to the higher observed deposition in treatment reach T1. The impact on channel change due to differences in riparian vegetation is worth exploring more in future studies since riparian vegetation type (e.g., grass versus trees) has been shown to influence the width of smaller stream channels [62–65].

Christensen et al. [48] found that treatment reach T1 demonstrated the highest channel–floodplain connectivity, defined as the interaction of water, sediment, and nutrients between

the channel and floodplain at high flow, compared to T2 and T3. They speculated that the higher connectivity resulted in higher rates of channel change, which was confirmed by the findings of this study. Further research is needed to establish the link between channel–floodplain connectivity and streambank erosion. DLS could be a valuable tool for such analysis due to its ability to measure channel morphology at high resolution, as demonstrated by this study.

4. Conclusions

The results of our study demonstrate the effectiveness of using drone-based lidar for measuring changes in channel morphology over time. A reach of Stroubles Creek, which underwent a restoration in 2010, was surveyed in 2010 and 2021 using a total station and in 2017 and 2021 using DLS. In spite of the limitations of NIR-based lidar in scanning channel bathymetry, the DLS-derived channel morphology metrics, such as cross-sectional area and width, showed good agreement with the same metrics calculated from the total station surveys. Total station surveying and DLS both have sources of bias or potential error; further analysis is needed to quantify and compare the uncertainty of each.

Compared to the total station survey, DLS was able to produce a much higher resolution measure of channel morphology with respect to both the number of cross sections and the number of points per cross section. This level of detail could allow for a more comprehensive assessment of reach-level changes in channel morphology following restoration that encourages the design of naturally dynamic channels. A common criticism of current restoration success criteria [8] is that they promote the design of static, single-thread channels. By providing detailed, site-scale topographic data, DLS surveys allow the assessment of more complex fluvial systems, such as zero-order and valley restoration designs [66,67].

Comparing the three treatment reaches, T3 (livestock exclusion, bank treatment, and inset floodplain) demonstrated the most stability from 2017 to 2021 compared to T1 (livestock exclusion) and T2 (livestock exclusion and bank treatment). Based on the channel morphology metrics, the DLS-derived cross sections in T3 had a median change closer to zero (with the exception of channel depth) and smaller variability in cross section change compared to the other two reaches. Additionally, it was observed from the high-resolution lidar DTMs that treatment reach T3 had the least erosion area and volume per reach length, indicating that livestock exclusion, inset floodplain creation, and riparian forest establishment provided the greatest channel stability post-restoration.

One area of future research identified by this study is the impact of riparian vegetation on ground classification errors during lidar data processing. While lidar can penetrate vegetation canopy to measure ground, classification errors persist. As previously discussed, dense vegetation can result in misclassified ground points. These errors result in uncertainty in the lidar-generated DTMs, which then propagate through to create uncertainty in the channel morphology metrics. In this study, the herbaceous vegetation in T1 could have resulted in higher ground classification errors than the woody vegetation in T2 and T3. These errors are expected to be more likely with denser riparian vegetation compared to the relatively sparse vegetation in this study. The impact on lidar data ground classification due to differences in riparian vegetation type and density as well as improved techniques to identify ground points should be explored more in future study.

On a final note, there is much more to stream restoration than just channel stability and channel change over time. The two main goals of the original restoration project were to “improve aquatic habitat” and “reduce sediment loading from eroding banks” [42]. The StREAM Lab at Virginia Tech has ongoing research in place to evaluate these goals. In this study, we only assessed channel change utilizing DLS. More research is needed to assess overall sediment budgets of the three treatments (versus simple average cross-section change) in this complex, human-impacted, natural experiment.

Author Contributions: Conceptualization, J.P.R.; data curation, C.H.; formal analysis, J.P.R.; funding acquisition, W.C.H. and T.W.-T.; methodology, J.P.R. and C.H.; supervision, W.C.H.; writing—original draft, J.P.R.; writing—review and editing, W.C.H. and T.W.-T. All authors have read and agreed to the published version of the manuscript.

Funding: This work was supported by the Virginia Agricultural Experiment Station (Blacksburg, VA, USA) and the U.S. Department of Agriculture (USDA) National Institute of Food and Agriculture (Washington, DC, USA).

Data Availability Statement: The 2021 drone lidar data presented in this study are openly available in OpenTopography at <https://doi.org/10.5069/G9348HK3> and opentopoID:OTDS.042023.6346.1.

Acknowledgments: The authors acknowledge the support of students, staff, and faculty associated with the Virginia Tech StREAM Lab (<https://vtstreamlab.weebly.com/> accessed on 1 March 2024), particularly Laura Lehmann for managing drone operations and lidar data collection.

Conflicts of Interest: The authors declare no conflicts of interest.

References

- Bernhardt, E.S.; Palmer, M.A.; Allan, J.D.; Alexander, G.; Barnas, K.; Brooks, S.; Carr, J.; Clayton, S.; Dahm, C.; Follstad-Shah, J.; et al. Synthesizing U.S. River Restoration Efforts. *Science* **2005**, *308*, 636–637. [[CrossRef](#)]
- Wheeler, T.B. Stream Restoration Techniques Draw Pushback. Available online: https://www.bayjournal.com/news/pollution/stream-restoration-techniques-draw-pushback/article_ffc96960-0895-11eb-b36f-efa466158524.html (accessed on 11 June 2023).
- Shields, F.D.; Copeland, R.R.; Klingeman, P.C.; Doyle, M.W.; Simon, A. Design for Stream Restoration. *J. Hydraul. Eng.* **2003**, *129*, 575–584. [[CrossRef](#)]
- Doll, B.A.; Grabow, G.L.; Hall, K.R.; Halley, J.; Harman, W.A.; Jennings, G.D.; Wise, D.E. *Stream Restoration: A Natural Channel Design Handbook*; NC Stream Restoration Institute, NC State University: Raleigh, NC, USA, 2003.
- Endreny, T.A.; Soulman, M.M. Hydraulic Analysis of River Training Cross-Vanes as Part of Post-Restoration Monitoring. *Hydrol. Earth Syst. Sci.* **2011**, *15*, 2119–2126. [[CrossRef](#)]
- Krymer, V.; Robert, A. Stream Restoration and Cribwall Performance: A Case Study of Cribwall Monitoring in Southern Ontario. *River Res. Appl.* **2014**, *30*, 865–873. [[CrossRef](#)]
- Buchanan, B.P.; Nagle, G.N.; Walter, M.T. Long-Term Monitoring and Assessment of a Stream Restoration Project in Central New York. *River Res. Appl.* **2014**, *30*, 245–258. [[CrossRef](#)]
- USACE. *Mitigation Banking Instrument (MBI) Monitoring Report Template*; Virginia Department of Environmental Quality: Richmond, VA, USA, 2023.
- Lave, R. The Controversy Over Natural Channel Design: Substantive Explanations and Potential Avenues for Resolution. *JAWRA J. Am. Water Resour. Assoc.* **2009**, *45*, 1519–1532. [[CrossRef](#)]
- Small, M.J.; Doyle, M.W. Historical Perspectives on River Restoration Design in the USA. *Prog. Phys. Geogr.* **2012**, *36*, 138–153. [[CrossRef](#)]
- Bash, J.S.; Ryan, C.M. Stream Restoration and Enhancement Projects: Is Anyone Monitoring? *Environ. Manag.* **2002**, *29*, 877–885. [[CrossRef](#)]
- Bernhardt, E.S.; Sudduth, E.B.; Palmer, M.A.; Allan, J.D.; Meyer, J.L.; Alexander, G.; Follstad-Shah, J.; Hassett, B.; Jenkinson, R.; Lave, R.; et al. Restoring Rivers One Reach at a Time: Results from a Survey of U.S. River Restoration Practitioners. *Restor. Ecol.* **2007**, *15*, 482–493. [[CrossRef](#)]
- Kondolf, G.M. Five Elements for Effective Evaluation of Stream Restoration. *Restor. Ecol.* **1995**, *3*, 133–136. [[CrossRef](#)]
- Kondolf, G.M.; Micheli, E.R. Evaluating Stream Restoration Projects. *Environ. Manag.* **1995**, *19*, 1–15. [[CrossRef](#)]
- Rubin, Z.; Kondolf, G.M.; Rios-Touma, B. Evaluating Stream Restoration Projects: What Do We Learn from Monitoring? *Water* **2017**, *9*, 174. [[CrossRef](#)]
- Lawler, D.M. The Measurement of River Bank Erosion and Lateral Channel Change: A Review. *Earth Surf. Process. Landf.* **1993**, *18*, 777–821. [[CrossRef](#)]
- Pyle, C.J.; Richards, K.S.; Chandler, J.H. Digital Photogrammetric Monitoring of River Bank Erosion. *Photogramm. Rec.* **1997**, *15*, 753–764. [[CrossRef](#)]
- Resop, J.P.; Hession, W.C. Terrestrial Laser Scanning for Monitoring Streambank Retreat: Comparison with Traditional Surveying Techniques. *J. Hydrol. Eng.* **2010**, *136*, 794–798. [[CrossRef](#)]
- Gatto, L.W. *Benchmark Design and Installation: A Synthesis of Existing Information*; Cold Regions Research and Engineering Laboratory (U.S.): Hanover, NH, USA, 1987.
- Hossain, M.A.; Gan, T.Y.; Baki, A.B.M. Assessing Morphological Changes of the Ganges River Using Satellite Images. *Quat. Int.* **2013**, *304*, 142–155. [[CrossRef](#)]
- Boothroyd, R.J.; Williams, R.D.; Hoey, T.B.; Barrett, B.; Prasojo, O.A. Applications of Google Earth Engine in Fluvial Geomorphology for Detecting River Channel Change. *WIREs Water* **2021**, *8*, e21496. [[CrossRef](#)]

22. Abbass, Z.D.; Maatooq, J.S.; Al-Mukhtar, M.M. Monitoring and Modelling Morphological Changes in Rivers Using RS and GIS Techniques. *Civ. Eng. J.* **2023**, *9*, 531–543. [[CrossRef](#)]
23. Legleiter, C.J.; Roberts, D.A. Effects of Channel Morphology and Sensor Spatial Resolution on Image-Derived Depth Estimates. *Remote Sens. Environ.* **2005**, *95*, 231–247. [[CrossRef](#)]
24. Legleiter, C.J. Mapping River Depth from Publicly Available Aerial Images. *River Res. Appl.* **2013**, *29*, 760–780. [[CrossRef](#)]
25. Woodget, A.S.; Austrums, R.; Maddock, I.P.; Habit, E. Drones and Digital Photogrammetry: From Classifications to Continuums for Monitoring River Habitat and Hydromorphology. *Wiley Interdiscip. Rev. Water* **2017**, *4*, e1222. [[CrossRef](#)]
26. Heritage, G.; Entwistle, N. Drone Based Quantification of Channel Response to an Extreme Flood for a Piedmont Stream. *Remote Sens.* **2019**, *11*, 2031. [[CrossRef](#)]
27. Diakakis, M.; Andreadakis, E.; Nikolopoulos, E.I.; Spyrou, N.I.; Gogou, M.E.; Deligiannakis, G.; Katsesiadou, N.K.; Antoniadis, Z.; Melaki, M.; Georgakopoulos, A.; et al. An Integrated Approach of Ground and Aerial Observations in Flash Flood Disaster Investigations. The Case of the 2017 Mandra Flash Flood in Greece. *Int. J. Disaster Risk Reduct.* **2019**, *33*, 290–309. [[CrossRef](#)]
28. Langhammer, J.; Lendziach, T.; Šolc, J. Use of UAV Monitoring to Identify Factors Limiting the Sustainability of Stream Restoration Projects. *Hydrology* **2023**, *10*, 48. [[CrossRef](#)]
29. Layzell, A.L.; Peterson, A.; Moore, T.L.; Bigham, K.A. UAS-Based Assessment of Streambank Stabilization Effectiveness in an Incised River System. *Geomorphology* **2022**, *408*, 108240. [[CrossRef](#)]
30. Kastridis, A.; Kirkenidis, C.; Sapountzis, M. An Integrated Approach of Flash Flood Analysis in Ungauged Mediterranean Watersheds Using Post-Flood Surveys and Unmanned Aerial Vehicles. *Hydrol. Process.* **2020**, *34*, 4920–4939. [[CrossRef](#)]
31. Dandois, J.P.; Ellis, E.C. Remote Sensing of Vegetation Structure Using Computer Vision. *Remote Sens.* **2010**, *2*, 1157–1176. [[CrossRef](#)]
32. Cavalli, M.; Tarolli, P.; Marchi, L.; Dalla Fontana, G. The Effectiveness of Airborne LiDAR Data in the Recognition of Channel-Bed Morphology. *CATENA* **2008**, *73*, 249–260. [[CrossRef](#)]
33. Anders, N.S.; Seijmonsbergen, A.C.; Bouten, W. Geomorphological Change Detection Using Object-Based Feature Extraction from Multi-Temporal LiDAR Data. *IEEE Geosci. Remote Sens. Lett.* **2013**, *10*, 1587–1591. [[CrossRef](#)]
34. Huang, C.; Peng, Y.; Lang, M.; Yeo, I.-Y.; McCarty, G. Wetland Inundation Mapping and Change Monitoring Using Landsat and Airborne LiDAR Data. *Remote Sens. Environ.* **2014**, *141*, 231–242. [[CrossRef](#)]
35. Tompalski, P.; Coops, N.C.; White, J.C.; Wulder, M.A.; Yuill, A. Characterizing Streams and Riparian Areas with Airborne Laser Scanning Data. *Remote Sens. Environ.* **2017**, *192*, 73–86. [[CrossRef](#)]
36. Resop, J.P.; Lehmann, L.; Hession, W.C. Drone Laser Scanning for Modeling Riverscape Topography and Vegetation: Comparison with Traditional Aerial Lidar. *Drones* **2019**, *3*, 35. [[CrossRef](#)]
37. Milan, D.J.; Heritage, G.L.; Hetherington, D. Application of a 3D laser scanner in the assessment of erosion and deposition volumes and channel change in a proglacial river. *Earth Surf. Process. Landf.* **2007**, *32*, 1657–1674. [[CrossRef](#)]
38. Resop, J.P.; Kozarek, J.L.; Hession, W.C. Terrestrial Laser Scanning for Delineating In-Stream Boulders and Quantifying Habitat Complexity Measures. *Photogramm. Eng. Remote Sens.* **2012**, *78*, 363–371. [[CrossRef](#)]
39. Brede, B.; Lau, A.; Bartholomeus, H.M.; Kooistra, L. Comparing RIEGL RICOPTRER UAV LiDAR Derived Canopy Height and DBH with Terrestrial LiDAR. *Sensors* **2017**, *17*, 2371. [[CrossRef](#)] [[PubMed](#)]
40. Backes, D.; Smigaj, M.; Schimka, M.; Zahs, V.; Grznárová, A.; Scaioni, M. River Morphology Monitoring of a Small-Scale Alpine Riverbed Using Drone Photogrammetry and Lidar. In *The International Archives of the Photogrammetry, Remote Sensing and Spatial Information Sciences*; Copernicus GmbH: Göttingen, Germany, 2020; Volume XLIII-B2-2020, pp. 1017–1024.
41. Islam, M.T.; Yoshida, K.; Nishiyama, S.; Sakai, K.; Tsuda, T. Characterizing Vegetated Rivers Using Novel Unmanned Aerial Vehicle-Borne Topo-Bathymetric Green Lidar: Seasonal Applications and Challenges. *River Res. Appl.* **2022**, *38*, 44–58. [[CrossRef](#)]
42. Wynn, T.; Hession, W.C.; Yagow, G. *Stroubles Creek Stream Restoration*; Virginia Department of Conservation and Recreation: Richmond, VA, USA, 2010; pp. 1–19.
43. Benham, B.; Brannan, K.; Dillaha, T.; Mostaghimi, S.; Wagner, R.; Wynn, J.; Yagow, G.; Zeckoski, R. *Benthic TMDL for Stroubles Creek in Montgomery County, Virginia*; Virginia Departments of Environmental Quality and Conservation and Recreation: Richmond, VA, USA, 2003; pp. 1–83.
44. Wynn-Thompson, T.; Hession, W.C.; Scott, D. StREAM Lab at Virginia Tech. *Resour. Mag.* **2012**, *19*, 8–9.
45. Abel, S.; Hopkinson, L.C.; Hession, W.C. Hydraulic and Physical Structure of Runs and Glides Following Stream Restoration. *River Res. Appl.* **2016**, *32*, 1890–1901. [[CrossRef](#)]
46. Prior, E.M.; Aquilina, C.A.; Czuba, J.A.; Pingel, T.J.; Hession, W.C. Estimating Floodplain Vegetative Roughness Using Drone-Based Laser Scanning and Structure from Motion Photogrammetry. *Remote Sens.* **2021**, *13*, 2616. [[CrossRef](#)]
47. Resop, J.P.; Lehmann, L.; Hession, W.C. Quantifying the Spatial Variability of Annual and Seasonal Changes in Riverscape Vegetation Using Drone Laser Scanning. *Drones* **2021**, *5*, 91. [[CrossRef](#)]
48. Christensen, N.D.; Prior, E.M.; Czuba, J.A.; Hession, W.C. Stream Restoration That Allows for Self-Adjustment Can Increase Channel-Floodplain Connectivity. *J. Ecol. Eng. Des.* **2024**, *1*. [[CrossRef](#)]
49. Hendrix, C.E. Evaluating the Long-Term Morphological Response of a Headwater Stream to Three Restoration Techniques. Master's Thesis, Virginia Polytechnic Institute and State University, Blacksburg, VA, USA, 2022.
50. Hession, W.C.; Lehmann, L.; Pingel, T.; Czuba, J.; Prior, B.; Christensen, N.; Kobayashi, Y.; Resop, J.P. *Virginia Tech StREAM Lab Winter 2021 Drone Lidar Survey*; OpenTopography: San Diego, CA, USA, 2021. [[CrossRef](#)]

51. Isenburg, M. *Processing Drone LiDAR from YellowScan's Surveyor, a Velodyne Puck Based System*; rapidlasso GmbH: Gilching, Germany, 2017.
52. YellowScan. YellowScan Surveyor: The Lightest and Most Versatile UAV LiDAR Solution. Available online: <https://www.yellowscan-lidar.com/products/surveyor/> (accessed on 21 March 2020).
53. Wheaton, J.M.; Brasington, J.; Darby, S.E.; Sear, D.A. Accounting for Uncertainty in DEMs from Repeat Topographic Surveys: Improved Sediment Budgets. *Earth Surf. Process. Landf.* **2010**, *35*, 136–156. [[CrossRef](#)]
54. Williams, R. DEMs of Difference. *Geomorphol. Tech.* **2012**, *2*, 1–17.
55. Okyay, U.; Telling, J.; Glennie, C.L.; Dietrich, W.E. Airborne Lidar Change Detection: An Overview of Earth Sciences Applications. *Earth-Sci. Rev.* **2019**, *198*, 102929. [[CrossRef](#)]
56. Fleming, P.M.; Merritts, D.J.; Walter, R.C. Legacy Sediment Erosion Hot Spots: A Cost-Effective Approach for Targeting Water Quality Improvements. *J. Soil Water Conserv.* **2019**, *74*, 67A–73A. [[CrossRef](#)]
57. Flener, C.; Vaaja, M.; Jaakkola, A.; Krooks, A.; Kaartinen, H.; Kukko, A.; Kasvi, E.; Hyyppä, H.; Hyyppä, J.; Alho, P. Seamless Mapping of River Channels at High Resolution Using Mobile LiDAR and UAV-Photography. *Remote Sens.* **2013**, *5*, 6382–6407. [[CrossRef](#)]
58. Abel, S.M. Near Boundary Turbulence Characteristics among Stream Restorations of Varying Intensity. Master's Thesis, West Virginia University, Morgantown, WV, USA, 2012.
59. Dietterick, B.C.; White, R.; Hilburn, R. Comparing LiDAR-Generated to Ground-Surveyed Channel Cross-Sectional Profiles in a Forested Mountain Stream. In Proceedings of the Coast Redwood Forests in a Changing California: A Symposium for Scientists and Managers, Santa Cruz, CA, USA, 21–23 June 2011; Gen. Tech. Rep. PSW-GTR-238. Pacific Southwest Research Station, US Forest Service: Albany, CA, USA, 2012; pp. 639–648.
60. Biron, P.M.; Choné, G.; Buffin-Bélanger, T.; Demers, S.; Olsen, T. Improvement of Streams Hydro-Geomorphological Assessment Using LiDAR DEMs. *Earth Surf. Process. Landf.* **2013**, *38*, 1808–1821. [[CrossRef](#)]
61. Ranganath, S.C.; Hession, W.C.; Wynn, T.M. Livestock Exclusion Influences on Riparian Vegetation, Channel Morphology, and Benthic Macroinvertebrate Assemblages. *J. Soil Water Conserv.* **2009**, *64*, 33–42. [[CrossRef](#)]
62. Trimble, S.W. Stream Channel Erosion and Change Resulting from Riparian Forests. *Geology* **1997**, *25*, 467–469. [[CrossRef](#)]
63. Hession, W.C.; Pizzuto, J.E.; Johnson, T.E.; Horwitz, R.J. Influence of Bank Vegetation on Channel Morphology in Rural and Urban Watersheds. *Geology* **2003**, *31*, 147–150. [[CrossRef](#)]
64. Anderson, R.J.; Bledsoe, B.P.; Hession, W.C. Width of Streams and Rivers in Response to Vegetation, Bank Material, and Other Factors. *JAWRA J. Am. Water Resour. Assoc.* **2004**, *40*, 1159–1172. [[CrossRef](#)]
65. Allmendinger, N.E.; Pizzuto, J.E.; Potter, N., Jr.; Johnson, T.E.; Hession, W.C. The Influence of Riparian Vegetation on Stream Width, Eastern Pennsylvania, USA. *GSA Bull.* **2005**, *117*, 229–243. [[CrossRef](#)]
66. Wheaton, J.M.; Bennett, S.N.; Bouwes, N.W.; Maestas, J.D.; Shahverdian, S.M. *Low-Tech Process-Based Restoration of Riverscapes: Design Manual*; Utah State University Restoration Consortium: Logan, UT, USA, 2019.
67. Forshay, K.J.; Weitzman, J.N.; Wilhelm, J.F.; Hartranft, J.; Merritts, D.J.; Rahnis, M.A.; Walter, R.C.; Mayer, P.M. Unearthing a Stream-Wetland Floodplain System: Increased Denitrification and Nitrate Retention at a Legacy Sediment Removal Restoration Site, Big Spring Run, PA, USA. *Biogeochemistry* **2022**, *161*, 171–191. [[CrossRef](#)]

Disclaimer/Publisher's Note: The statements, opinions and data contained in all publications are solely those of the individual author(s) and contributor(s) and not of MDPI and/or the editor(s). MDPI and/or the editor(s) disclaim responsibility for any injury to people or property resulting from any ideas, methods, instructions or products referred to in the content.